Raman spectroscopy of the charge-orbital ordering in layered manganites

K. Yamamoto
Department of Applied Physics, University of Tokyo, Tokyo 113-8656, Japan

T. Kimura
Joint Research Center for Atom Technology (JRCAT), Tsukuba 305-0046, Japan

T. Ishikawa* and T. Katsufuji†
Department of Applied Physics, University of Tokyo, Tokyo 113-8656, Japan

Y. Tokura
Department of Applied Physics, University of Tokyo, Tokyo 113-8656, Japan
and Joint Research Center for Atom Technology (JRCAT), Tsukuba 305-0046, Japan
(Received 3 August 1999; revised manuscript received 25 October 1999)

The lattice and electronic response in the course of concomitant charge and orbital-ordering transition has been investigated for single crystals of layered manganites, single-layered $La_{0.5}Sr_{1.5}MnO_4$, and bilayered $LaSr_2Mn_2O_7$, by Raman-scattering spectroscopy. In the charge-orbital-ordered state ($T<217$ K for $La_{0.5}Sr_{1.5}MnO_4$ and ~ 100 K$<T<210$ K for $LaSr_2Mn_2O_7$), four phonon modes are activated in the MnO_2 plane, indicating the existence of both Jahn-Teller type and breathing mode type lattice distortions. The diffuse scattering response with B_{1g} symmetry is suppressed in the charge-orbital-ordered state, both for $La_{0.5}Sr_{1.5}MnO_4$ and $LaSr_2Mn_2O_7$, signaling that the fluctuation caused by the dynamical charge-orbital correlation is suppressed in the charge-orbital-ordered state. These features reveal the unique nature of the charge-orbital-ordering transition realized by the complex interplay of charge and orbital degrees of freedom.

I. INTRODUCTION

There is growing interest in charge-ordering phenomena in transition metal oxide systems such as $La_2NiO_{4+\delta}$,[1,2] $La_{2-x}Sr_xNiO_{4+\delta}$,[3,4] $La_{2-x-y}Nd_ySr_xCuO_4$,[5–7] and also in manganites.[8–14] The current interest arises not only from the importance of the ''electron-crystallization'' in the strongly correlated electron systems, but also from the possible relevance to novel mechanisms of high-temperature superconductivity in the cuprates and colossal magnetoresistance (CMR) in the manganites.[15,16] In particular, the charge ordering in the manganites is closely correlated with the orbital degree of freedom,[17] which arises from doubly degenerate e_g state of conduction electron. Such a cooperative orbital-ordering produces not only local and asymmetric lattice distortion due to the Jahn-Teller effect, but also macroscopic lattice strain. Thus, the various phenomena in manganite systems occur as a result of complex interplay of charge, spin, lattice, and orbital degrees of freedom.

By narrowing the one-electron bandwidth, or reducing the electronic dimension from the prototypical double exchange system, e.g., $La_{1-x}Sr_xMnO_3$, the ferromagnetic metal phase is destabilized, and instead a charge-ordered state tends to appear at low temperatures. In Fig. 1 are depicted crystal structures of Ruddlesden-Popper series manganites, (a) $La_{0.5}Sr_{1.5}MnO_4$ and (b) $LaSr_2Mn_2O_7$, with inherent charge-ordering instability. As seen in the figure, these crystals with the general formula $(La,Sr)_{n+1}Mn_nO_{3n+1}$ are composed of n-MnO_2 layers separated by a $(La,Sr)_2O_2$ blocking layer. $La_{0.5}Sr_{1.5}MnO_4$ with $n=1$ and with hole doping level of $x=1/2$, is one of the most typical charge-ordering system among the manganites. Recent electron-diffraction[12] and neutron-diffraction[18] measurements on $La_{0.5}Sr_{1.5}MnO_4$ have confirmed the onset of charge ordering at $T_{CO}=217$ K and spin ordering at $T_N=110$ K, confirming the formation of the so-called CE-type spin structure. Its resistivity steeply rises below around 220 K in accord with the onset of the charge ordering.[12] The checker-board-like ordering of Mn^{3+}/Mn^{4+} sites and the $d_{3x^2-r^2}/d_{3y^2-r^2}$-type orbital-ordered state as shown in Fig. 1(d) have been directly evidenced by the resonant x-ray diffraction below T_{CO}.[19] For $LaSr_2Mn_2O_7$ with $n=2$, on the other hand, a reentrant feature shows up for the charge-orbital-ordered state. At first, the $d_{3x^2-r^2}/d_{3y^2-r^2}$-type orbital ordering at Mn^{3+} sites occurs accompanying the checker-board-like ordering of the Mn^{3+}/Mn^{4+} sites [Fig. 1(d)] below $T_{CO}\sim 210$ K. With the decrease of temperature, the CE-type spin ordering sets in at around 145 K. However, the ordering turns into a layer-type (A-type) antiferromagnetic below ~ 100 K with the ferromagnetic spin ordering within the constituent single layer, accompanied by the disappearance of charge-orbital and CE-type spin ordering.[13,14,20,21] The transition from the charge-orbital-ordered state to the A-type antiferromagnetic phase is of the first order as evidenced by the hystereses in resistivity[14] and in the superlattice-peak intensity observed by diffraction measurements.[20,21] The A-type antiferromagnetic ground state has been interpreted as due to the ''ferromagnetic'' ordering of the $d_{x^2-y^2}$-type orbital.[22–24] This situation seems to be quite generic for the highly doped (around $x=0.5$) manganites. Notably, interaction along the c axis (z direction) in the $d_{x^2-y^2}$-type orbital ordered state is absent for the single layer compound, whereas, it is present but

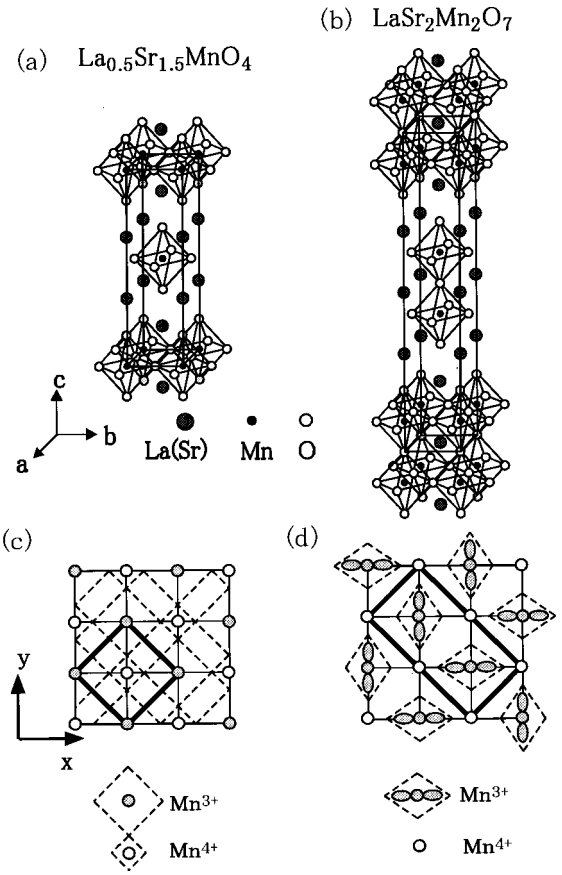

FIG. 1. The crystal structures of (a) $La_{0.5}Sr_{1.5}MnO_4$ with MnO_2 single-layer units and (b) $LaSr_2Mn_2O_7$ with MnO_2 bilayer units. Possible unit cells (enclosed by thick solid lines) of (c) a charge-ordered state with simple breathing-mode-type lattice distortion with $P4/mmm$ symmetry, where the volume of the unit cell is doubled from those of the original structures [(a) and (b)] and (d) a charge-orbital-ordered state with Jahn-Teller distortion around Mn^{3+} sites with $Pmam$ symmetry, where the volume of the unit cell is quadrupled from those of the original ones. Dotted lines represent deformed Mn-O_6 octahedra.

restricted within the double-layer unit for the bilayer manganite. This may give rise even a more complex feature for the bilayer manganite than the corresponding pseudocubic manganites.

To investigate the possible novel interplay of charge and orbit with lattice dynamics in the course of phase transitions, we have performed Raman-scattering measurements, using single crystals of $La_{0.5}Sr_{1.5}MnO_4$ and $LaSr_2Mn_2O_7$, where little deviation from the original crystal structure with $I4/mmm$ symmetry [Figs. 1(a) and 1(b)] has been detected by the diffraction measurements. As confirmed by studies in the pseudocubic perovskite system $La_{1-x}Sr_xMnO_3$,[25,26] Raman-scattering is a very sensitive probe of local or dynamical structural change. Furthermore, by electronic Raman response, we can derive the information about the low-energy electronic excitations including their symmetries. So far, Raman-scattering studies on these layered manganites have been reported for the insulator to metal transition in compositionally adjacent bilayer compound $La_{1.2}Sr_{1.8}Mn_2O_7$ ($x=0.4$),[27–29] which has the ground state of ferromagnetic metal. In this study, we will reveal the characteristic change of lattice (orbital) and charge dynamics in the course of concomitant charge-orbital-ordering transition by Raman spectroscopy. The presently obtained results can also be the basis of the assignment of charge-orbital correlation which are likely relevant to the CMR physics.

II. EXPERIMENTAL PROCEDURE

The samples studied in this work are single crystals grown by the floating zone method,[12,14,30] and have the tetragonal $I4/mmm$ symmetry [Figs. 1(a) and 1(b)] at room temperature. In Raman measurements for the ab planes, we cleaved the crystals just prior to the measurement and used such a cleaved flat surface of the ab plane. As for the measurement for the ac plane, we have cut and polished to the optical flatness. To remove possible stress of the polished ac plane surface, we annealed the crystal in O_2 atmosphere at a temperature of 950 °C for 100 h, although we found that there was little difference in the temperature dependence and the line shapes of the Raman spectra between the annealed ac plane and as-polished ac plane. A 514.5-nm light from an argon ion laser (less than 20 mW) was focused into a 0.1-mm-diameter spot. The temperature values referred to in this paper are the nominal ones inside the cryostat. Comparing Stokes and anti-Stokes spectra, we estimated the rise of temperature caused by the local laser heating that does not exceed 10 K at 120 K, which is around the transition temperature for $LaSr_2Mn_2O_7$.[31] Spectra were measured in four polarization configurations $(x'x')=(x+y,x+y)$, $(x'y')=(x+y,x-y)$, (xy), and (zz); the notation x or y represents the polarization of incident or scattered light along the in-plane Mn-O direction, and z represents the direction of c axis of the crystals, i.e., the direction of the out of plane Mn-O bond. Each polarization spectrum is composed of $A_{1g}+B_{2g}$, $B_{1g}+A_{2g}$, $B_{2g}+A_{2g}$, and A_{1g} respectively, which are irreducible representations of the space group $I4/mmm$, i.e., the tetragonal form of these compounds. The A_{2g} component is likely to be much weaker than A_{1g} and B_{1g} components.[32] We have also measured the Raman spectra in the (zx) polarization configuration that corresponds to the E_g symmetry. We found that the spectral intensity of (zx) is less than about 25% that of (zz) spectra and observed no phonon peaks except for leak of the A_{1g} modes in (zz) configuration with very tiny spectral intensity, both in $La_{0.5}Sr_{1.5}MnO_4$ and $LaSr_2Mn_2O_7$. Therefore, we have neglected the A_{2g} and E_g component in the following discussion of this paper.

III. EXPERIMENTAL RESULTS AND DISCUSSIONS

A. Overall feature of Raman spectra and mode assignment

Figure 2 shows the Raman spectra for $La_{0.5}Sr_{1.5}MnO_4$ with (a) $(x'x')$ and $(x'y')$ configuration, (c) (zz) configuration, and for $LaSr_2Mn_2O_7$ with (b) $(x'x')$ and $(x'y')$, and (d) (zz) configuration. What we will discuss below are two spectral features; phonon peaks with large scattering intensity in a charge-orbital-ordered state, as seen in the lower panel of Fig. 2(a), and the middle panel of Fig. 2(b), and diffuse scattering in a lower-frequency region of Raman spectra ($\leqslant 300$ cm^{-1}), as seen at the top panel of Figs. 2(a), 2(b), and 2(d).

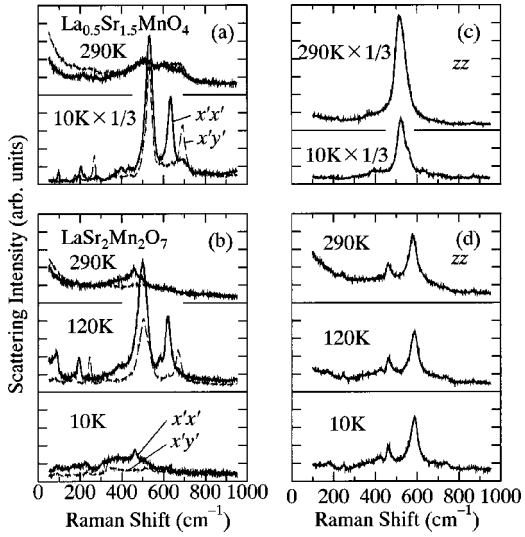

FIG. 2. (a) In-plane and (c) out-of-plane Raman spectra of paramagnetic insulating phase (290 K) and charge-orbital-ordered state (10 K) of a single-layer compound $La_{0.5}Sr_{1.5}MnO_4$. The panels (b) and (d) show in-plane and out-of-plane Raman spectra of $LaSr_2Mn_2O_7$, respectively, in paramagnetic insulating phase (290 K), charge-orbital-ordered phase (120 K), and layer-type (A-type) antiferromagnetic phase (10 K).

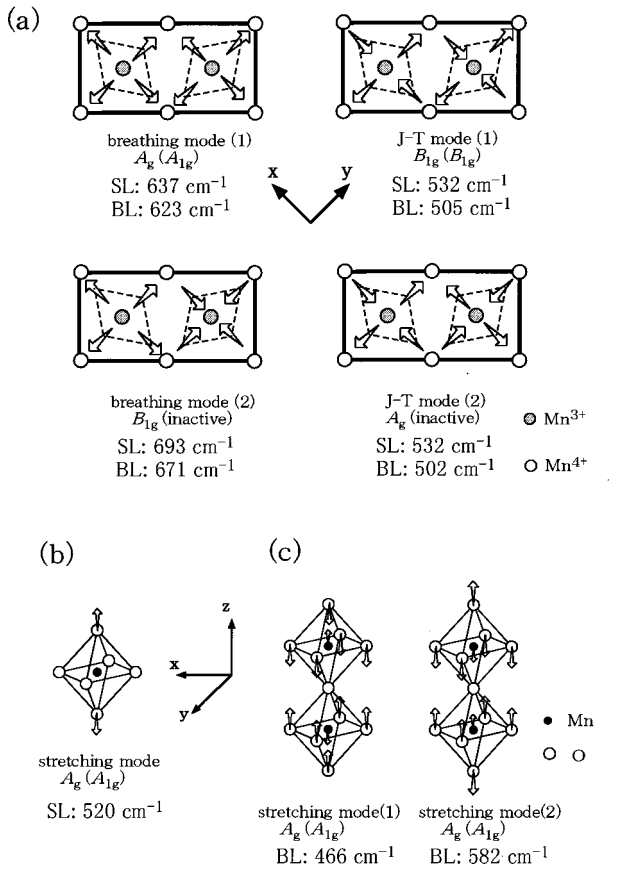

FIG. 3. (a) In-plane Raman active modes in the charge-orbital-ordered states, and out-of-plane modes with out-of-plane Mn-O stretching motion of (b) $La_{0.5}Sr_{1.5}MnO_4$ and (c) $LaSr_2Mn_2O_7$. Each mode is named tentatively in this study. Symmetries of the modes described out of parentheses are the one corresponding to the unit cell described in Fig. 1(d) and those in parentheses to the simple charge-ordering model shown in Fig. 1(c). The observed energies of the Raman peaks, which are assigned to the respective modes and also indicated for $La_{0.5}Sr_{1.5}MnO_4$ (SL), and $LaSr_2Mn_2O_7$ (BL). As for assignment, see the text.

First, let us focus on the phonon peaks. The Raman spectra in the prototypical charge-orbital-ordered state [Fig. 1(d)] in the single-layer manganite $La_{0.5}Sr_{1.5}MnO_4$ are exemplified in the lower panel of Fig. 2(a), where four phonon modes are observed with large scattering intensities, at 532 and 637 cm^{-1} for the $(x'x')$ polarization, and at 532 and 693 cm^{-1} for the $(x'y')$ polarization. The original structure with tetragonal $I4/mmm$ symmetry [Fig. 1(a)] allows four Raman active modes $(2A_{1g}+2E_g)$, but they should not be observed for the ab-plane polarizations. Since these peaks quickly increase their intensity just below T_{CO}, as will be later discussed in more detail, they can be assigned to the phonon modes activated by the lattice distortion upon the charge-orbital ordering. There also are several tiny phonon peaks at 97, 204, 280, 395, 436, and 695 cm^{-1} for the $(x'x')$ polarization, and at 176, 196, 268, 360, 434, 594, and 635 cm^{-1} for the $(x'y')$ polarization. Though their temperature dependences are not as clear as those of the major peaks, they can be also the phonon modes activated by the lattice distortion upon the charge-orbital ordering.

Let us focus on four major peaks appearing in the charge-orbital ordered state. From their fairly large scattering intensities, they must be reflecting the major lattice distortion in the charge-orbital ordered state. From their rather large energies $(500-700\ cm^{-1})$, they are likely assigned to the in-plane Mn-O bond stretching modes. Since the detailed crystal structure and symmetry in the charge-orbital ordered state is unknown, we will show from the group theoretical point of view that both breathing modes and Jahn-Teller type modes are likely responsible for these phonon peaks with assumption of the lattice distortion depicted in Fig. 1(d). This lattice distortion taking account of the cooperative Jahn-Teller distortion is the most probable one in such a charge-orbital-ordered state for $La_{0.5}Sr_{1.5}MnO_4$ as demonstrated by the resonant x-ray scattering study. Since none of the infrared active modes coincide with the activated Raman peak energies,[33] they are expected to be phonon modes characteristic of the charge-orbital-ordered state. First, let us consider the case of the alternate breathing distortion [Fig. 1(c)] that is probable in the simple ''charge''-ordered state. This unit cell has the symmetry with $P4/mmm$, and its volume is doubled from the original unit cell [Fig. 1(a)].[34] With this unit cell, 12 modes $(4A_{1g}+B_{1g}+2B_{2g}+5E_g$, except for one A_{2g} mode)[35] become Raman active. Among them, we expect that three modes $(A_{1g}+2B_{2g})$ be observed in the $(x'x')$ polarization and one B_{1g} mode in the $(x'y')$ polarization. In this case, the A_{1g} and B_{1g} modes correspond to a breathing mode (1) and a Jahn-Teller (JT-) type mode (1), respectively, as depicted in Fig. 3(a). However, it is obvious that the lattice model of Fig. 1(c) is not enough for explanation of the number of observed phonon modes with B_{1g} symmetry in the layered manganites, even if we consider only the major phonon peaks. We have to assume the unit cell with the cooperative Jahn-Teller distortion [Fig. 1(d)] as may be realized in the concomitantly charge and orbital ordered state of $La_{0.5}Sr_{1.5}MnO_4$.[19] Such a lattice distortion is present in other

TABLE I. The frequencies (in the unit of cm^{-1}) of the observed phonon peaks in the charge-orbital-ordered state of $La_{0.5}Sr_{1.5}MnO_4$ (10 K) and $LaSr_2Mn_2O_7$ (120 K) in in-plane polarization. Also shown are the numbers of the observed phonon peaks and the expected ones with their corresponding symmetry in the respective unit cells depicted in Figs. 1(c) (CO) and 1(d) (CO/OO). The numbers in parentheses are for the number of the major phonon peaks.

		$La_{0.5}Sr_{1.5}MnO_4$		$LaSr_2Mn_2O_7$	
		$(x'x')$	$(x'y')$	$(x'x')$	$(x'y')$
		97	176	85	173
		204	196	195	248
		280	268	390	310
		395	360	502	330
		436	434	581	433
		532	532	623	505
		637	594		532
		695	635		621
			693		671
observed		8	9	6	9
		(2)	(2)	(2)	(2)
expected	CO	3	1	at least 5	4
	$P4/mmm$	$A_{1g}+2B_{2g}$	B_{1g}	$4B_{2g}$ + at least[a] $1A_{1g}$	$4B_{1g}$
	CO/OO	at least 3	9	at least 2	14
	$Pmam$	at least $3A_g$	$9B_{1g}$	at least $2A_g$	$14B_g$

[a]See Ref. 37.

charge-orbital-ordering system with the checker-board-like ordering of Mn^{3+}/Mn^{4+} sites and the $d_{3x^2-r^2}/d_{3y^2-r^2}$-type orbital-ordered state, such as perovskite-type manganites $Pr_{0.5}Ca_{0.5}MnO_3$ (Ref. 9) and $La_{0.5}Ca_{0.5}MnO_3$.[38] In the present case, the unit cell becomes orthorhombic $Pmam$ symmetry,[36] and 39 modes $(11A_g+9B_{1g}+8B_{2g}+11B_{3g})$ become Raman active. Among the activated modes [at least three A_g modes[37] and all of B_{1g} modes are expected to be observed in the $(x'x')$ and $(x'y')$ configurations, respectively], we can choose four modes as reflecting both the breathing type and JT lattice distortion. Two of them are the breathing mode (1) and the JT mode (1) [see Fig. 3(a)], corresponding to the modes discussed above, but their symmetries turn to A_g and B_{1g}. Other two modes in this deformed lattice are also depicted in Fig. 3(a) as a breathing mode (2) with B_{1g} symmetry and a JT mode (2) with A_g symmetry. We can consider that the breathing mode (1) and the JT mode (1) are activated by the lattice distortion upon the ''charge'' ordering alone, while the breathing mode (2) and the JT mode (2) are activated by the *concomitant* charge-orbital ordering. Concerning the plausible frequencies of these modes, we can refer to the lattice dynamical calculation (LDC) on $LaMnO_3$, which gives the frequencies of the modes corresponding to the JT and breathing modes as about 580 and 670 cm^{-1}, respectively.[39] On the bases of above discussions on the symmetry of phonon modes and the result of LDC, we can assign phonon peaks at 532 and 637 cm^{-1} in the $(x'x')$ spectrum of $La_{0.5}Sr_{1.5}MnO_4$ [Fig. 3(a)] to the JT mode (2) and the breathing mode (1) and phonon peaks at 532 and 693 cm^{-1} in the $(x'y')$ spectrum to the JT mode (1) and the breathing mode (2), respectively. Table I summarizes the frequencies and the number of activated phonon peaks in the in-plane polarized Raman spectra of $La_{0.5}Sr_{1.5}MnO_4$, as well as the expected number of phonon modes both for the unit cell for merely ''charge''-ordered state [Fig. 1(c)] and charge-orbital-ordered state [Fig. 1(d)] together with their symmetry.

The in-plane spectra of $LaSr_2Mn_2O_7$ (bilayer structure) in the charge-orbital-ordered state at 120 K [Fig. 2(b)] quite resemble those of $La_{0.5}Sr_{1.5}MnO_4$. Two modes are observed in the $(x'x')$ polarization spectrum at 502 and 623 cm^{-1}, and other two modes are observed for the $(x'y')$ polarization at 505 and 671 cm^{-1}. These four Raman modes almost disappear above $T_{CO}\sim 210$ K and more importantly in the *A*-type antiferromagnetic phase below ~ 100 K as exemplified by the 10 K spectra of Fig. 2(b). Among ten Raman allowed modes $(4A_{1g}+B_{1g}+5E_g)$ in the original structure with tetragonal $I4/mmm$ symmetry [Fig. 1(b)], only one B_{1g} mode, perhaps corresponding to the sharp phonon peak observed at 330 cm^{-1} in $(x'y')$ configuration of the ab plane spectra, can show up in the ab plane spectra.[40] Therefore, we can also regard these four modes in a region of 500 -700 cm^{-1} as phonon modes reflecting the order parameter of the concomitant charge-orbital ordering. The resemblance to the in-plane Raman spectra for $La_{0.5}Sr_{1.5}MnO_4$ indicates that the Raman spectra of $LaSr_2Mn_2O_7$ are determined by the lattice distortion within a MnO_2 layer whose pattern of lattice distortion within ab plane in the charge-orbital-ordered state are expected to be the same as that of $La_{0.5}Sr_{1.5}MnO_4$.[14,21] This and the reasons described below allow us the same mode assignment to the phonon peaks for $LaSr_2Mn_2O_7$ in the charge-orbital-ordered state, namely, peaks at 502 and 623 cm^{-1} in the $(x'x')$ spectrum to JT mode (2) and breathing mode (1), and peaks at 505 and 671 cm^{-1} in the $(x'y')$ spectrum to JT mode (1) and breathing mode (2), respectively (see Fig. 2). In order to confirm that

the Raman spectra of $LaSr_2Mn_2O_7$ is mostly determined by the lattice distortion within a MnO_2 layer, and to show that the four phonon modes in Fig. 3(a) can also appear in the Raman spectra with the same polarization configurations as those in the single-layer case, we first examine the expected phonon modes in the bilayer compound, and then, discuss the symmetry of the four modes in the bilayer case.

According to electron[13] and x-ray[14,21] diffraction studies, the coupling along the *c* axis within a bilayer unit is in phase. Furthermore, a recent x-ray study[41] has revealed that the ''herring bones'' of the orbital ordering direct the same direction between the adjacent bilayer units. The space group of the charge or charge-orbital-ordered state corresponding to Figs. 1(c) and 1(d) are $P4/mmm$ and $Pmam$, respectively. According to the factor group analysis for the bilayer case, the expected numbers of the phonon modes in the unit cells in Figs. 1(c) and 1(d) are 22 $(9A_{1g} + 4B_{1g} + 4B_{2g} + 5E_g$, except for $3A_{2g})$ and 66 $(17A_g + 14B_{1g} + 15B_{2g} + 20B_{3g})$, respectively. The expected number of phonon modes in the bilayer case increases (for in-plane mode, see the number of B_{1g} modes that represents only that of the in-plane modes) from the single-layer case in both unit cells.

This is contrary to the present Raman result (see also Table I), where the number of the major phonon modes does not increase. These confirm that the number of the in-plane phonon peaks in $LaSr_2Mn_2O_7$, especially for major peaks, is almost determined by the symmetry of a MnO_2 layer; that is, the effect of the interlayer interaction of the modes within a bilayer unit hardly appears in the in-plane Raman spectra.

Obviously, however, the four modes within each layer within a bilayer unit should not be completely independent of those in the counter layer for the symmetry of the unit cell. Since the interlayer mode coupling seems to be weak in this case, the activated in-plane phonon modes in $LaSr_2Mn_2O_7$ is composed of the in-phase and out-of-phase linear combination of the mode within each MnO_2 layer that is described by the in-plane mode for $La_{0.5}Sr_{1.5}MnO_4$ in Fig. 3(a). The modes between two layers within a bilayer unit should be the same owing to the symmetry of the unit cell. The in-phase coupling of the atomic motion between two layers yields a mode with the same symmetry (polarization dependence) as that of $La_{0.5}Sr_{1.5}MnO_4$; for example, breathing mode (1) in $La_{0.5}Sr_{1.5}MnO_4$ with A_g symmetry can also be breathing mode (1) with A_g symmetry in $LaSr_2Mn_2O_7$. On the other hand, the out-of-phase coupling yields an IR active mode, or optical inactive mode; for example, the combination of two breathing mode (1)s becomes a B_{1u} mode. Thus, in the bilayer compound, each symmetry of the modes in Fig. 3(a) remains the same as those for single layer compound, and the increased four modes are IR active modes, or optical inactive modes.[42] This explains why the four modes in Fig. 3(a) can also be observed in the Raman spectra of the bilayer $LaSr_2Mn_2O_7$ as four phonon peaks with the same symmetry as those in $La_{0.5}Sr_{1.5}MnO_4$.

There are also observed several tiny peaks at 85, 195, 390, and 581 cm^{-1}, for the $(x'x')$ polarization and at 173, 248, 310, 433, 532, and 621 cm^{-1} for the $(x'y')$ polarization. They also can be considered to be the activated modes as well by the lattice distortion induced by the charge-orbital ordering, although the detailed assignments are not made.

The phonon peaks observed in the (zz) configuration, on the other hand, are classified into two cases: Raman allowed modes in the original structure with tetragonal $I4/mmm$ symmetry, and activated modes by the lattice distortion upon the charge-orbital ordering. The two phonon modes at 222 and 520 cm^{-1} in the single-layer compound $La_{0.5}Sr_{1.5}MnO_4$ are assigned to the two A_{1g} modes expected in the original structure: the peak at 222 cm^{-1} is assigned to the motion along the *c* direction of rare-earth–alkaline-earth ions and the other at 520 cm^{-1} with large intensity is to the motion of out-of-plane oxygen [described as a stretching mode in Fig. 3(b)]. The other modes at 290, 401, 560, 630, and 710 cm^{-1} are characteristic of the charge-orbital-ordered state. The two major modes observed in the bilayer $LaSr_2Mn_2O_7$ at 466 and 582 cm^{-1} are also the Raman-allowed modes in the original structure with tetragonal $I4/mmm$ symmetry, and are assigned to the stretching mode (1) and stretching mode (2), respectively, as depicted in Fig. 3(c). Among the rest of the modes with tiny intensities, two modes at 178 and 247 cm^{-1} are also assigned to the Raman allowed modes in the original structure: the atomic motion of rare-earth–alkaline earth ions along the *c* direction. The rest of the modes at 362, 420, 683, and 740 cm^{-1} may be the activated modes by the lattice distortion upon the charge-orbital ordering.

Then let us turn our eyes to the diffuse-scattering feature in the lower-energy part ($\leqslant 300$ cm^{-1}). The diffuse scattering are observed for in-plane spectra both of single-layer and bilayer compounds $La_{0.5}Sr_{1.5}MnO_4$ and $LaSr_2Mn_2O_7$ and only for out-of plane spectra of $LaSr_2Mn_2O_7$ [see Figs. 2(a), 2(b), and 2(d)]. Comparing Stokes and anti-Stokes spectra, we confirmed that they arise from the Raman process. These features are reminiscent of the electronic Raman process in metals that arises from the strongly incoherent carrier motion described by the collision limited model.[43–47] In these layered manganites, however, the values of resistivity are rather insulating (of the order of $10^{-1}-10^{0}$ Ω cm) even in the paramagnetic phase above T_{CO}. Therefore, it is unlikely that such an electronic Raman process as in conventional metals with well-defined Fermi surface,[48] where the incident light is scattered by the energy density fluctuation of electron with anisotropic mass tensor, is applicable to this case. The diffuse scattering part as observed in the present Raman spectra is likely to arise from the fluctuation of the real-space charge-spin density, and that with B_{1g} symmetry is reflecting the locally anisotropic one caused by dynamical correlation of charge orbital, as will be evidenced by the following subsections.

B. Charge-orbital ordering transition in $La_{0.5}Sr_{1.5}MnO_4$

On the basis of the mode assignment established as above, we argue the lattice dynamics in the course of charge-orbital-ordering transition as well as the dynamical charge-orbital correlation. Figure 4 shows the temperature dependence of Raman spectra of $La_{0.5}Sr_{1.5}MnO_4$; (a) the diffuse-scattering part in $(x'x')$, $(x'y')$, and (xy) configurations, and the phonon peaks in (d) $(x'x')$ and (e) $(x'y')$ configurations.

The four phonon modes appearing in Figs. 4(d) and 4(e) are the ones we have assigned to the finger print of the concomitant charge-orbital ordering. These peaks are observed even at 290 K as broad structures, perhaps due to the sub-

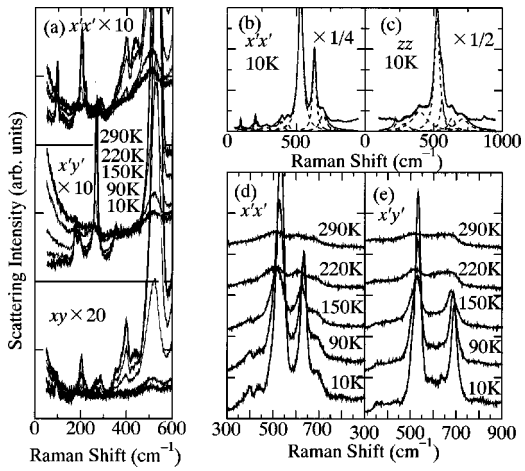

FIG. 4. Temperature dependence of Raman spectra for $La_{0.5}Sr_{1.5}MnO_4$. Panel (a) shows the diffuse-scattering part with $(x'x')$, $(x'y')$, and (xy) configuration. Panels (b) and (c) show the results of curve fitting for Raman spectra in $(x'x')$ and (zz) configuration, respectively. The fitting curve (solid line) is composed of a relaxational component (broken curve) and Lorentzian oscillators (dotted curves). Panels (d) and (e) show the temperature dependence of phonon peaks in $(x'x')$ and $(x'y')$ configurations, respectively.

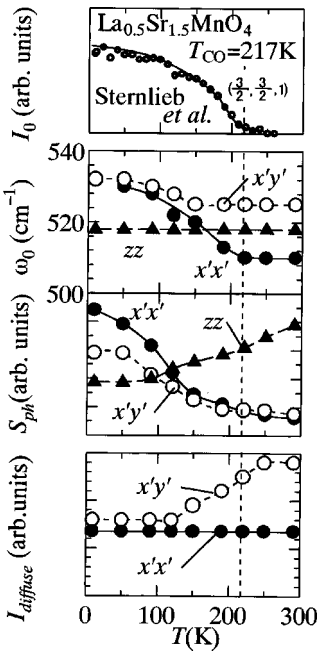

FIG. 5. Temperature (T) dependence of peak energies (ω_0) and intensities ($S_{\rm ph}$) of phonon modes (the second and third panels from the top, respectively). Open circles, filled circles, and filled triangles correspond to peak energies and intensities of Jahn-Teller mode (1), Jahn-Teller mode (2), and stretching mode (see also Fig. 3). The bottom panel shows the intensity ($I_{\rm diffuse}$) of diffuse scattering with $(x'x')$ (filled circles) and $(x'y')$ (open circles) configuration. The temperature dependence of the neutron diffraction intensity (I_0) of the $(\frac{3}{2},\frac{3}{2},1)$ peak due to the charge ordering is shown on the top panel for comparison.

sisting charge-orbital correlation above $T_{\rm CO}$, but suddenly increases their intensities below $T_{\rm CO}$. The larger scattering intensity of JT modes than those of breathing modes perhaps may relate to a difference in the amplitudes of breathing-type and Jahn-Teller distortion in the charge-orbital-ordered state. In fact, a LDA calculation concludes that Jahn-Teller distortion is about eight times larger than that of breathing-mode type.[49] Incidentally, the phonon peak at 520 cm^{-1} in the (zz) configuration [see, Fig. 2(c)] monotonically decreases in intensity with the decrease of temperature.

Next, let us scrutinize the temperature dependence of the diffuse-scattering part by Fig. 4(a). The scattering intensity decreases with the decrease of temperature, but that of $(x'y')$ configuration is different from those of $(x'x')$ and (xy). In crossing $T_{\rm CO}=217$ K (220 to 150 K), the crystal shows larger reduction of the scattering intensity for $(x'y')$ configuration than for $(x'x')$ and (xy). This can clearly be observed in Fig. 2(a): the intensity of diffuse scattering of $(x'y')$ configuration obviously exceeds that of $(x'x')$ at 290 K, but becomes comparable or even smaller at 10 K. The temperature dependence of these scattering parts are affected, and hence should be corrected, by the Bose-thermal factor, yet the above features remain transparent after this correction.

In order to discuss the quantitative aspect, we have fit the $(x'x')$, $(x'y')$, and (zz) Raman spectra with Lorentzian oscillators for the phonon part, and with the relaxational form for the lower-energy diffuse scattering part, the latter of which is based on the fluctuation-dissipation theorem in the case of strong damping

$$I(\omega,T)=\frac{1}{1-\exp(-\hbar\omega/kT)}\times\left(\frac{I_{\rm diffuse}\omega\Gamma}{\omega^2+\Gamma^2}+\sum_{i=1}^{m}\frac{S_i\omega\gamma_i}{(\omega^2-\omega_i^2)^2+\omega^2\gamma_i^2}\right). \quad (1)$$

Here, ω is the Raman shift, $I_{\rm diffuse}$ the symmetry-dependent scattering amplitude, Γ the scattering rate, and ω_i, γ_i, and S_i correspond to the frequency, width, and intensity of each phonon mode. We have fixed $\Gamma=80$ cm^{-1} for in-plane $(x'x')$ and $(x'y')$ spectra because of large arbitrariness in deciding it, and hence can only compare the change in scattering amplitude $I_{\rm diffuse}$. As for the out-of-plane (zz) spectra, we fixed $I_{\rm diffuse}=0$. The result of the curve fitting is exemplified in Figs. 4(b) and 4(c). The Lorentzian curve fitting other than the major phonon peaks is only to reproduce the experimental results better.

Figure 5 shows the temperature dependence of the fitting parameters. There is also displayed the temperature dependence of the superlattice peak $(\frac{3}{2},\frac{3}{2},1)$ intensity for the charge ordering that is concomitant with the orbital ordering.[18] The temperature dependence of peak energy of in-plane modes [JT mode (1) and JT mode (2)] and out-of-plane mode (stretching mode) shows a contrastive behavior (see, the second panel in Fig. 5) although these commonly correspond to the modes with the length modulation of Mn-O bonds. The peak energies of in-plane Mn-O stretching modes increases below $T_{\rm CO}$, while that of out-of-plane Mn-O stretching mode (assigned to stretching mode) shows little temperature dependence. Such a selective hardening of the in-plane Mn-O mode may reflect the in-plane directional ordering of the e_g orbital, such as $d_{3x^2-r^2}/d_{3y^2-r^2}$ [see Fig. 1(d)], and resultant change in bond covalency upon the charge-orbital ordering.

A difference in temperature dependence between in-plane and out-of-plane modes are also seen in the phonon spectral intensity (see the third panel from the top in Fig. 5). The activated intensity of the in-plane modes that reflects the order parameter of charge-orbital ordering increases below T_{CO}, while that of out-of-plane mode monotonically decreases, as if the spectral intensity were transferred from an out-of-plane mode to in-plane modes. The change of phonon spectral intensities in the course of the charge-orbital ordering may arise from two mechanisms: One is the activation due to the lowering of the local symmetry, and the other is the change of the bond character [the change of absorption coefficient or dielectric constant in the relevant energy region (2.4−2.5 eV) of the incident and scattered lights is minimal with change of temperature[30]]. Obviously, the Raman signal intensity for the in-plane Mn-O modes corresponds to the former case and can be used as a local and dynamical probe of the charge-orbital ordering or correlation. The observed activation of the in-plane mode subsisting above T_{CO} is a clear indication of (perhaps two-dimensional) dynamical charge-orbital ordering. The behavior is contrastive with the behavior of the superlattice peak intensity (the top panel of Fig. 5) that only probes the average symmetry. On the other hand, the out-of-plane Mn-O stretching mode phonon in (zz) configuration is originally Raman-active in the regular tetragonal lattice. The degrease in its intensity in the course of the charge-orbital-ordering transition is due to the second mechanism. Namely, the in-plane directional ordering of the e_g orbital decreases the $d_{3z^2-r^2}$ character of the out-of-plane Mn-O bonding, and hence reduces its coupling with the electronic state.

As for the in-plane diffuse scattering responses, they show the clear symmetry-dependent variation with temperature. The scattering intensity of the $(x'x')$ configuration (dominantly composed of $A_{1g}+B_{2g}$) scarcely varies, while that of $(x'y')$ configuration (dominantly composed of B_{1g}) decreases just below T_{CO}, and becomes constant around T_N. We confirmed that the intensity of (xy) configuration (dominantly composed of B_{2g}) shows no temperature dependence, either. Therefore, only the B_{1g} component shows the temperature dependence. The plausible origin for the diffuse scattering response with B_{1g} symmetry is the spin density fluctuation, or a novel fluctuation correlated with dynamical correlation of charge and orbital. The relation between the diffuse scattering response with B_{1g} symmetry and the dynamical correlation of charge and orbital is clearly evidenced by the broadened but well-subsisting feature above T_{CO} of the phonon peaks which can be assigned to the finger print of the concomitant charge and orbital ordering at lower ($T < T_{CO}$) temperatures. The scattering intensity arising from such a microscopic process should decrease in accordance with the onset of the charge-orbital ordering, and become constant below T_N, where the long-range charge-orbital ordering almost completes and the fluctuation is suppressed.[50]

C. Reentrant charge-orbital ordering transition in $LaSr_2Mn_2O_7$

Figure 6 shows the temperature dependence of Raman spectra of $LaSr_2Mn_2O_7$, in which a reentrant behavior of the charge-orbital ordered state is observed; (a) the diffuse scattering part in $(x'x')$, $(x'y')$, and (xy) configuration, and the phonon peaks in (d) $(x'x')$ and (e) $(x'y')$ configurations, respectively.

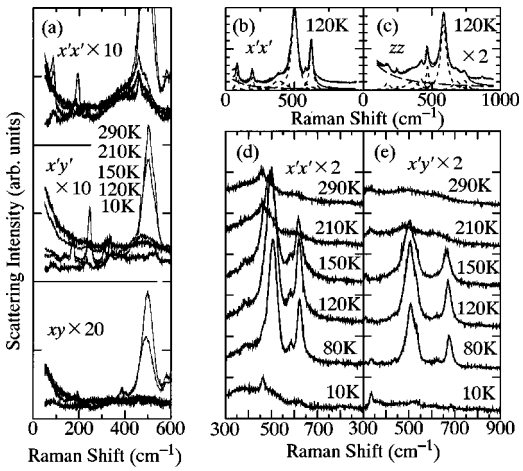

FIG. 6. Temperature dependence of Raman spectra of $LaSr_2Mn_2O_7$. Panel (a) shows the diffuse scattering part with $(x'x')$, $(x'y')$, and (xy) configuration. Panels (b) and (c) show the results of curve fitting of Raman spectra in $(x'x')$ and (zz) configuration, respectively. The fitting curve (solid line) is composed of relaxational component (a broken curve) and Lorentzian oscillators (dotted curves). Panels (d) and (e) show the temperature dependence of phonon peaks in $(x'x')$ and $(x'y')$ configuration, respectively.

First, let us focus on the temperature dependence of the phonon peaks. The four phonon peaks in the $(x'x')$ and $(x'y')$ configuration can be seen even at 290 K as broad structures, indicating the existence of dynamical charge-orbital correlation above T_{CO}. With the decrease of temperature below T_{CO}, they quickly gain their intensity. With further decreasing temperature, say, below 100 K, the spectral intensity rather decreases and then almost disappears at enough low temperatures, e.g., at 10 K. It has recently been confirmed by electron, x-ray, and neutron-diffraction studies that the charge-orbital ordered state with CE-type antiferromagnetic spin structure melts again below about 100 K (Refs. 13,14,20,21) to the *A*-type antiferromagnetic state with the ferromagnetic spin arrangement within the constituent single layers. The observed temperature dependence of these four phonon peaks confirms that these modes are reflecting the order parameter of charge-orbital ordering. The larger intensities of JT modes than those of breathing modes indicate again that the major lattice distortion is Jahn-Teller type, as in the case of single-layer compound. A sharp tiny peak at 466 cm^{-1} in $(x'x')$ configuration, which remains to the lowest temperature, corresponds to the stretching mode (1) in the (zz) configuration and is observed for in-plane polarization perhaps due to the existence of structural modulation even in the *A*-type antiferromagnetic phase. The energies and intensity of phonon peaks in the (zz) configuration, which are originally Raman active, shows little change in the course of successive phase transition with decreasing temperature, contrary to the case of the single-layer $La_{0.5}Sr_{1.5}MnO_4$.

The temperature dependence of in-plane diffuse scattering [Fig. 6(a)] shows quite an analogous feature to the case of the single-layer compound. The scattering intensity of

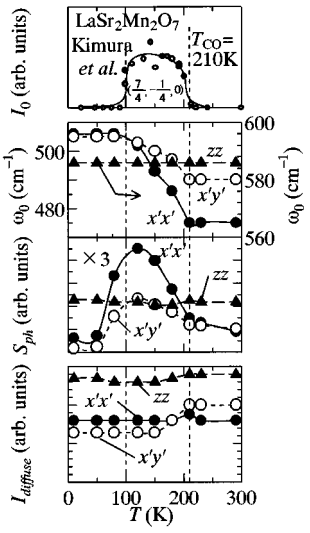

FIG. 7. Temperature (T) dependence of peak energies (ω_0) and intensities ($S_{\rm ph}$) of phonon modes (the second and third panel from the top, respectively). Open circles, filled circles, and filled triangles correspond to peak energies and amplitudes of Jahn-Teller mode (1), Jahn-Teller mode (2), and stretching mode (2) (see also Fig. 3). The bottom panel shows the intensity ($I_{\rm diffuse}$) of diffuse scattering with $(x'x')$ (filled circles), $(x'y')$ (open circles), and (zz) (filled triangles) configuration. The temperature dependence of the x-ray diffraction intensity (I_0) of the $(\frac{7}{4},-\frac{1}{4},0)$ peak due to the orbital ordering is also shown on the top panel for comparison.

$(x'y')$ configuration considerably decreases with the decrease of temperature below $T_{\rm CO}$ ($=$ 210 K), but those of $(x'x')$ and (xy) do not [see also the top and second panels in Fig. 2(b)]. The intensity of diffuse scattering of $(x'y')$ configuration is slightly larger than that of $(x'x')$ at 290 K, but at 120 K and also at 10 K, the intensity for $(x'x')$ configuration rather exceeds that of $(x'y')$.

We fitted the in-plane and out-of-plane spectra with Eq. (1) to discuss the temperature dependence of these components more quantitatively. For the diffuse scattering part, we have fixed $\Gamma = 80$ cm^{-1} for in-plane $(x'x')$ and $(x'y')$ spectra, and $\Gamma = 100$ cm^{-1} for (zz) spectra. The discrepancy between the values of Γ for in-plane and out-of-plane may arise from the difference of the damping mechanism, but we will not discuss this any longer, because of large arbitrariness in deciding them. We will only discuss the temperature dependence of total magnitudes ($I_{\rm diffuse}$) for the diffuse-scattering part. The result of the curve fitting is exemplified in Figs. 6(b) and 6(c).

The temperature dependence of the fitting parameters are shown in Fig. 7. The second and the third panels from the top represent the temperature dependence of peak energies and intensities of the phonon modes, respectively. The bottom panel shows the temperature dependence of the intensities of the diffuse-scattering part of the respective configuration spectra. On the top panel of Fig. 7, we also display, for comparison, the temperature dependence of x-ray diffraction $(\frac{7}{4},-\frac{1}{4},0)$ peak intensity corresponding to the orbital ordering.[14] The intensity of in-plane phonon modes [JT mode (1) and (2)] goes almost parallel with that of the x-ray-scattering intensity probing the orbital ordering, as expected, apart from the two-dimensional correlation above $T_{\rm CO}$ seen in the phonon modes. The peak energies of these modes monotonically increases below $T_{\rm CO}$, and saturate in the A-type antiferromagnetic phase where the phonon peaks almost disappear. It is worth noting here that the activated phonon modes gradually disappears below 100 K, but without being broadened significantly, as seen in Figs. 6(d) and 6(e). This makes sharp contrast with the broadening behavior of phonon peaks above $T_{\rm CO}$. According to a recent neutron-diffraction study,[20] the A-type antiferromagnetic phase sets in around 210 K and undergoes the reentrant transition. Since the phase transition between the A-type antiferromagnetic phase and the charge-orbital-ordered state around 100 K is typically of the first order, even in the intervening charge-orbital-ordered state there coexists the A-type antiferromagnetic phase, as evidenced by a recent neutron-diffraction study.[20] Likewise, the fragment of the charge-orbital-ordered region appears to still survives in the reentrant A-type phase region below 100 K: The correlation length of charge-orbital-ordering monotonically decreases down to 50 K with decreasing temperature.[41] The remnant of the in-plane phonon peaks [JT modes (1), (2), etc.] below 100 K reflects such a microscopic charge-orbital-ordered domain in A-type antiferromagnetic phase. From their difference in phonon peak widths between A-type antiferromagnetic phase below 100 K and paramagnetic phase above $T_{\rm CO}$, we can speculate that the charge-orbital ordering is frozen as the fragment of the charge-orbital-ordered state embedded in the A-type antiferromagnetic phase, contrary to the case above $T_{\rm CO}$, where the charge-orbital correlation is expected to be dynamical and shortlived.

As for the out-of-plane stretching mode (2) (at 582 cm^{-1}) in the (zz) configuration, not only the peak energy but also the intensity are almost temperature independent, contrary to the corresponding out-of-plane mode of the single-layer compound. This difference between the single-layer case and the bilayer one may arise from the bond characters of the out-of-plane Mn-O bond above $T_{\rm CO}$. In the bilayer compound, the out-of-plane Mn-O bond length is already compressed at room temperature and the ratio of the bond length of out-of-plane Mn-O to in-plane one is unchanged between room temperature and 10 K.[51] This crystal environment already stabilizes the $d_{x^2-y^2}$ character of e_g electron of Mn^{3+} site, and reduces the $d_{3z^2-r^2}$ character even well above $T_{\rm CO}$. The weaker out-of-plane Mn-O bonding leads to the reduced coupling of the out-of-plane stretching modes with the electronic state that determines the phonon spectral intensity. Thus, irrespective of the ordering of e_g orbital below $T_{\rm CO}$, the coupling of the out-of-plane stretching modes with the electronic state remains weak, giving rise to the temperature-independent spectral intensity of stretching mode (2).

Finally, let us briefly discuss the temperature dependence of the intensities of diffuse scattering. As for the in-plane components, they show a parallel behavior with those of the single-layer case: The scattering intensity of the $(x'x')$ and (zz) configuration (dominantly composed of $A_{1g}+B_{2g}$ and A_{1g} component, respectively) scarcely varies, while that of $(x'y')$ configuration (almost consists of B_{1g} component) decreases just below $T_{\rm CO}$, and becomes constant around T_N. We also confirmed that the scattering intensity of (xy) configuration shows essentially no variation with temperature. Therefore, as in the single-layer compound, the dynamical

correlation of the charge-orbital ordering may cause the fluctuation with B_{1g} symmetry above T_{CO}.

IV. CONCLUSION

We have measured Raman spectra of the layered manganites $La_{0.5}Sr_{1.5}MnO_4$ and $LaSr_2Mn_2O_7$, showing the charge-orbital-ordering transitions. In both systems, the activated phonon modes with large scattering intensities are observed in the charge-orbital-ordered state for the in-plane polarizations; two modes with A_{1g} symmetry, and other two with B_{1g} symmetry. They are considered to be activated by concomitant charge and orbital-ordering accompanying both breathing-mode type and Jahn-Teller-type lattice distortions. The intensity of these in-plane Mn-O bond stretching modes shows almost parallel temperature dependence to that of the superlattice diffraction peaks caused by the charge-orbital ordering, although the dynamical charge-orbital correlation above T_{CO} is also clearly sensed by the remnant intensity and broadened profile of these phonon peaks. These phonon modes show appreciable hardening below T_{CO}, perhaps due to the change in the in-plane Mn-O bond character in the orbital ordered state. On the other hand, the out-of-plane Mn-O bond stretching modes do not show hardening with decrease of temperature and their intensities temperature independent (for the bilayer compound), or rather weakened (for the single-layer one). This indicates that the coupling of out-of-plane Mn-O mode with the electronic state is weakened due to the directional ordering of e_g orbital within the ab plane.

The diffuse-scattering response dominantly with B_{1g} symmetry is suppressed in the course of charge-orbital ordering, both for $La_{0.5}Sr_{1.5}MnO_4$ and $LaSr_2Mn_2O_7$. The suppression of diffuse scattering starts just below T_{CO}, and completes around T_N, where the long-range order of charge and orbital is almost fully developed. On the other hand, diffuse scattering with other symmetries (A_{1g} and B_{2g}) are temperature independent. Such a diffuse-scattering response with B_{1g} symmetry is likely to arise not from the electronic Raman process in conventional metals but from the spin density fluctuation or a locally anisotropic fluctuation caused by the *dynamical* correlation of charge and orbital.

ACKNOWLEDGMENTS

We thank N. Nagaosa and E. Saitoh for helpful discussions. The present work was supported by a Grant-In-Aid for Scientific Research from Ministry of Education, Science, Sports and Culture, Japan, and by NEDO.

*Present address: Department of Applied Physics, Tokyo Institute of Technology, Tokyo 152-8551, Japan.

†Present address: Department of Advanced Materials Science, University of Tokyo, Tokyo 113-8656, Japan.

[1] J. M. Tranquada, D. J. Buttrey, V. Sachan, and J. E. Lorenzo, Phys. Rev. Lett. **73**, 1003 (1994).

[2] J. M. Tranquada, J. E. Lorenzo, D. J. Buttrey, and V. Sachan, Phys. Rev. B **52**, 3581 (1995).

[3] C. H. Chen, S-W. Cheong, and A. S. Cooper, Phys. Rev. Lett. **71**, 2461 (1993).

[4] S.-H. Lee and S-W. Cheong, Phys. Rev. Lett. **79**, 2514 (1997).

[5] J. M. Tranquada, B. J. Sternlieb, J. D. Axe, Y. Nakamura, and S. Uchida, Nature (London) **375**, 561 (1995).

[6] J. M. Tranquada, J. D. Axe, N. Ichikawa, Y. Nakamura, S. Uchida, and B. Nachumi, Phys. Rev. B **54**, 7489 (1996).

[7] J. M. Tranquada, J. D. Axe, N. Ichikawa, A. R. Moodenbaugh, Y. Nakamura, and S. Uchida, Phys. Rev. Lett. **78**, 338 (1997).

[8] C. H. Chen and S-W. Cheong, Phys. Rev. Lett. **76**, 4042 (1996).

[9] Z. Jirak, S. Krupicka, Z. Simsa, M. Dlouha, and S. Vratislav, J. Magn. Magn. Mater. **53**, 153 (1985).

[10] Y. Tomioka, A. Asamitsu, H. Kuwahara, Y. Moritomo, and Y. Tokura, Phys. Rev. B **53**, R1689 (1995).

[11] H. Kuwahara, Y. Tomioka, A. Asamitsu, Y. Moritomo, and Y. Tokura, Science **270**, 961 (1995).

[12] Y. Moritomo, Y. Tomioka, A. Asamistu, Y. Tokura, and Y. Matsui, Phys. Rev. B **51**, 3297 (1995).

[13] J. Q. Li, Y. Mastui, T. Kimura, and Y. Tokura, Phys. Rev. B **57**, R3205 (1998).

[14] T. Kimura, R. Kumai, Y. Tokura, J. Q. Li, and Y. Matsui, Phys. Rev. B **58**, 11 081 (1998).

[15] Y. Tokura, H. Kuwahara, Y. Moritomo, Y. Tomioka, and A. Asamitsu, Phys. Rev. Lett. **76**, 3184 (1996).

[16] P. Shiffer, A. P. Ramirez, W. Bao, and S-W. Cheong, Phys. Rev. Lett. **75**, 3336 (1995).

[17] T. Kimura, Y. Tomioka, A. Asamitsu, and Y. Tokura, Phys. Rev. Lett. **81**, 5920 (1998).

[18] B. J. Sternlieb, J. P. Hill, U. C. Wildgruber, G. M. Luke, B. Nachumi, Y. Moritomo, and Y. Tokura, Phys. Rev. Lett. **76**, 2169 (1996).

[19] Y. Murakami, H. Kawada, H. Kawata, M. Tanaka, T. Arima, Y. Moritomo, and Y. Tokura, Phys. Rev. Lett. **80**, 1932 (1998).

[20] M. Kubota, H. Yoshizawa, Y. Moritomo, H. Fujioka, K. Hirota, and Y. Endoh, J. Phys. Soc. Jpn. **68**, 2202 (1999).

[21] T. Chatterji, G. J. McIntyre, W. Caliebe, R. Suryanarayanan, G. Dhalenne, and A. Revcolevschi, Phys. Rev. B **61**, 570 (2000).

[22] T. Mizokawa and A. Fujimori, Phys. Rev. B **56**, R493 (1997).

[23] R. Maezono, S. Ishihara, and N. Nagaosa, Phys. Rev. B **58**, 11 583 (1998).

[24] H. Kuwahara, T. Okuda, Y. Tomioka, A. Asamitsu, and Y. Tokura, Phys. Rev. Lett. **82**, 4316 (1999).

[25] M. V. Abrashev, A. P. Litvinchuk, M. N. Iliev, R. L. Meng, V. N. Popov, V. G. Ivanov, R. A. Chakalov, and C. Thomsen, Phys. Rev. B **59**, 4146 (1999).

[26] M. V. Abrashev, V. G. Ivanov, M. N. Iliev, R. A. Chakalov, R. I. Cakalova, and C. Thomsen, Phys. Status Solidi B **215**, 631 (1999).

[27] D. B. Romero, V. B. Podobedov, A. Weber, J. P. Rice, J. F. Mitchell, R. P. Sharma, and H. D. Drew, in *Science and Technology of Magnetic Oxides*, edited by M. F. Hundley, J. H. Nickel, R. Ramesh, and Y. Tokura (Materials Research Society, Pittsburgh, 1998), Vol. 494, p. 305.

[28] D. B. Romero, V. B. Podobedov, A. Weber, J. P. Rice, J. F. Mitchell, R. P. Sharma, and H. D. Drew, Phys. Rev. B **58**, R14 737 (1998).

[29] K. Yamamoto, T. Kimura, T. Ishikawa, T. Katsufuji, and Y. Tokura, J. Phys. Soc. Jpn. **68**, 2538 (1999).

[30] T. Ishikawa, K. Ookura, and Y. Tokura, Phys. Rev. B **59**, 8367 (1999).

[31] Especially in the strongly correlated electron systems, the simple estimate of temperature using Stokes and anti-Stokes is not always justified. In the present systems, however, we have confirmed that Stokes spectra coincide with anti-Stokes spectra after dividing out Bose factor at 290 and at 200 K, where the local heating effect is expected to be less serious. Therefore, we can expect that the simple relation between Stokes and anti-Stokes spectra is not a bad approximation in these systems in evaluating the local temperature raise. We thus confirmed that the local heating effect by laser is not so serious even at around transition temperatures as to affect our following discussions.

[32] The scattering intensity of (xy) polarization spectra does not exceed, at most, 50% of those of $(x'x')$ and $(x'y')$ configuration spectra. In the energy range of Raman shift that we have measured, A_{2g} component is usually much weaker than B_{2g} component for two-dimensional spin systems such as Gd_2CuO_4 [P. E. Sulewski, P. A. Fleury, K. B. Lyons, and S-W. Cheong, Phys. Rev. Lett. **67**, 3864 (1991)]. Therefore, it is anticipated that neglecting it scarcely affects the following discussions.

[33] The peak energies of IR active phonon for $La_{0.5}Sr_{1.5}MnO_4$ at 10 K are, 170, 268, 286, 347, 380, 427, 568, and 621 cm^{-1} (tetragonal E_u modes in origin), 225, 283, 372, 403, and 489 cm^{-1} (tetragonal A_{2u} modes in origin) (Ref. 30). For $LaSr_2Mn_2O_7$, 163, 213, 293, 350, and 602 cm^{-1} (tetragonal E_u modes in origin), and 172, 196, 348, and 490 cm^{-1} (tetragonal A_{2u} modes in origin) [T. Ishikawa, T. Kimura, Y. Moritomo, K. Tobe, T. Katsufuji, K. Ookura, and Y. Tokura (unpublished)]. Increase in the number of the modes is due to the lowered symmetry in the charge-orbital-ordered state.

[34] With this unit cell, the site symmetry of Mn site is D_{4h} and atomic motion is absent in the Raman active modes. As for in-plane O site, which has C_{2v} site symmetry, the atomic motion is confined in xy plane for B_{1g} mode, and also for B_{2g} modes.

[35] We have neglected one A_{2g} mode activated in this unit cell, for it does not affect the following discussions. Since A_{2g} phonon modes are usually not Raman active, and in this layered manganite, there is no apparent A_{2g} mode in the Raman spectra; the A_{2g} phonon mode is expected to be observed both in $(x'y')$ and (xy) spectra, but not in $(x'x')$, while no such a phonon peak is present in the actual spectra.

[36] With this unit cell, Mn^{3+} site has C_{2h} site symmetry and its atomic motion is absent in the Raman active modes. For Mn^{4+} and in-plane O site, they have C_{2v} and C_s site symmetries respectively, and atomic motions for B_{1g} modes are commonly confined in xy plane.

[37] The reason why not all A_g (or A_{1g}) modes are observed in-plane is that, there are A_g (or A_{1g}) modes originate from the tetragonal A_{1g} modes whose atomic motion is only along the c axis, and not observed in the in-plane polarization. For example, in the single-layer manganite case with the unit cell in Fig. 1(d) whose volume is quadrupled from the original unit cell, there can be eight modes whose atomic motion is along the c axis.

[38] P. G. Radaelli, D. E. Cox, M. Marezio, and S.-W. Cheong, Phys. Rev. B **55**, 3015 (1997).

[39] M. N. Iliev, M. V. Abrashev, H.-G. Lee, V. N. Popov, Y. Y. Sun, C. Thomsen, R. L. Meng, and C. W. Chu, Phys. Rev. B **57**, 2872 (1998).

[40] According to the factor group analysis, the tetragonal $I4/mmm$ structure allows four A_{1g} Raman active modes, one B_{1g} mode, and five E_g modes. All these Raman active modes are not to be observed except for the B_{1g} mode that is assigned to the sharp phonon peak observed around 330 cm^{-1} in $(x'y')$ spectra (Refs. 27 and 28). Thus none of these intense and broad phonon peaks observed in the charge-orbital-ordered state correspond to the Raman active modes in the undistorted original structure.

[41] Y. Wakabayashi, Y. Murakami, I. Koyama, T. Kimura, Y. Tokura, Y. Moritomo, K. Hirota, and Y. Endoh (unpublished).

[42] The symmetry of the modes arising from the linear combination of the phonon modes in the single-layer compound in Fig. 3(a) is as follows: linear combinations of breathing mode $(1)s$ become A_g+B_{1u} modes, those of breathing mode $(2)s$ become $B_{1g}+A_u$ modes, those of JT mode $(1)s$ and JT mode $(2)s$ yield $B_{1g}+A_u$, and A_g+B_{1u} modes, respectively.

[43] M. Chandrasekhar, M. Cardona, and E. O. Kane, Phys. Rev. B **16**, 3679 (1977).

[44] G. Conreras, A. K. Sood, and M. Cardona, Phys. Rev. B **32**, 924 (1985).

[45] I. P. Ipatova, A. V. Subashiev, and V. A. Voitenko, Solid State Commun. **37**, 893 (1981).

[46] A. Zawadowski and M. Cardona, Phys. Rev. B **42**, 10 732 (1990).

[47] A. Virosztek and J. Ruvalds, Phys. Rev. B **45**, 347 (1992).

[48] M. V. Klein, in *Light Scattering in Solids*, edited by M. Cardona and G. Güntherrodt (Springer-Verlag, Berlin, 1983), Vol. I, p. 147.

[49] I. Solovyev and K. Terakura (unpublished).

[50] Such a suppression of the diffuse scattering with B_{1g} symmetry is also observed in bilayer $LaSr_2Mn_2O_7$, as will be discussed later. This temperature dependence of the diffuse scattering reminds us of that of electronic Raman scattering in the course of metal (conventional)-to-insulator transition, where the diffuse scattering described by the collision limited model is expected to be suppressed in an insulator phase. However, we should point out here our result of recent Raman-scattering measurement executed on compositionally adjacent bilayer compound $La_{1.2}Sr_{1.8}Mn_2O_7$ $(x=0.4)$, where the insulator-to-metal transition is observed around Curie temperature (T_C) (Ref. 29). We have found that the diffuse scattering with B_{1g} symmetry observed in the paramagnetic insulating phase is rather suppressed in the ferromagnetic metallic phase below T_C. Such a temperature dependence is closely correlated with the dynamical charge-orbital correlation that is evidenced by the activated phonon peaks above T_C, but suppressed in the ferromagnetic metallic phase below T_C. Thus, in layered manganites, the suppression of the diffuse scattering with B_{1g} symmetry is observed not only in the charge-orbital-ordered insulator phase, but also in the ferromagnetic metallic phase. Therefore, this suppression cannot be considered to correspond to the opening of a charge gap in the [100] or [010] direction, but should be considered to the suppression of the fluctuation caused by a dynamical charge-orbital correlation.

[51] M. Kubota, H. Fujioka, K. Hirota, K. Ohoyama, Y. Moritomo, H. Yoshizawa, and Y. Endoh (unpublished).